JOURNAL OF TISSUE ENGINEERING AND REGENERATIVE MEDICINE
J Tissue Eng Regen Med 2011; **5**: e52–e62.
Published online 23 September 2010 in Wiley Online Library (wileyonlinelibrary.com) **DOI:** 10.1002/term.336

RESEARCH ARTICLE

Efficient *in vivo* vascularization of tissue-engineering scaffolds

Anja Hegen[1†], Anna Blois[1†], Crina E. Tiron[1], Monica Hellesøy[1], David R. Micklem[1], Jacques E. Nör[4], Lars A. Akslen[2,3] and James B. Lorens[1]*

[1]*Department of Biomedicine, University of Bergen, N-5009 Bergen, Norway*
[2]*The Gade Institute, Section for Pathology, University of Bergen, N-5009 Bergen, Norway*
[3]*Department of Pathology, Haukeland University Hospital, N-5021 Bergen, Norway*
[4]*School of Dentistry and Department of Otolaryngology, University of Michigan, Ann Arbor, MI 48109-1078, USA*

Abstract

The success of tissue engineering depends on the rapid and efficient formation of a functional blood vasculature. Adult blood vessels comprise endothelial cells and perivascular mural cells that assemble into patent tubules ensheathed by a basement membrane during angiogenesis. Using individual vessel components, we characterized intra-scaffold microvessel self-assembly efficiency in a physiological *in vivo* tissue engineering implant context. Primary human microvascular endothelial and vascular smooth muscle cells were seeded at different ratios in poly-L-lactic acid (PLLA) scaffolds enriched with basement membrane proteins (Matrigel) and implanted subcutaneously into immunocompromised mice. Temporal intra-scaffold microvessel formation, anastomosis and perfusion were monitored by immunohistochemical, flow cytometric and *in vivo* multiphoton fluorescence microscopy analysis. Vascularization in the tissue-engineering context was strongly enhanced in implants seeded with a complete complement of blood vessel components: human microvascular endothelial and vascular smooth muscle cells *in vivo* assembled a patent microvasculature within Matrigel-enriched PLLA scaffolds that anastomosed with the host circulation during the first week of implantation. Multiphoton fluorescence angiographic analysis of the intra-scaffold microcirculation showed a uniform, branched microvascular network. 3D image reconstruction analysis of human pulmonary artery smooth muscle cell (hPASMC) distribution within vascularized implants was non-random and displayed a preferential perivascular localization. Hence, efficient microvessel self-assembly, anastomosis and establishment of a functional microvasculture in the native hypoxic *in vivo* tissue engineering context is promoted by providing a complete set of vascular components.

Received 5 March 2010; Accepted 20 May 2010

Supporting information may be found in the online version of this article.

Keywords **angiogenesis; scaffold; endothelial; mural cell; microcirculation; multiphoton**

1. Introduction

Tissue engineering endeavours to replace and restore organ function to treat end-stage disease. The success of tissue engineering strategies depends on the efficient formation of a functional blood vasculature to serve the metabolic needs of bioengineered tissues. However, contemporary tissue-engineering approaches are hampered by inadequate vascularization of the hypoxic engineered microenviroment that debilitates tissue development (Muschler *et al*., 2004; Patterson *et al*., 2008). Inclusion of angiogenesis-stimulating factors can improve scaffold vascularization; however, this process is slow and difficult to control (Lazarous *et al*., 1996) Formation of new blood vessels requires cell–cell and cell–matrix interactions

*Correspondence to: James B. Lorens, Department of Biomedicine, University of Bergen, Jonas Lies Vei 91, N-5009 Bergen, Norway. E-mail: jim.lorens@biomed.uib.no
† *These authors contributed equally to this study.*

between blood vessel components; endothelial cells mural cells (vascular smooth muscle cells, pericytes) and vascular basement membrane that collectively regulate vessel assembly (Black *et al*., 1998, 1999; Nguyen and D'Amore, 2001). Mural cells define a context comprising heterotypic cell–cell contact, extracellular matrix (ECM) deposition and soluble factors that inhibit endothelial proliferation, maintain capillary diameter, regulate blood flow and provide survival signals for the cells in the blood vessel (Hall, 2006; Kutcher and Herman, 2009). Heterotypic cell–cell contacts at interdigitations between endothelial cells and mural cells provide a unique presentation context for paracrine factors such as VEGF and angiopoietins, which regulate endothelial cell responses (Darland and D'Amore, 1999). Hence, the generation of tissue-engineered microvascular networks in three-dimensional (3D) matrices, utilizing only vessel-derived endothelial cells (ECs) or ECs differentiated from progenitor cell populations, will depend on the recruitment of host-derived mural cells, such as vascular smooth muscle cells (SMCs) for proper vessel maturation (Kaully *et al*., 2009). Studies with implanted endothelial spheroids demonstrated that the investment of engineered vessels by host mural cells enhances their stability (Alajati *et al*., 2008; Wenger *et al*., 2005). Alternatively, ectopic expression of anti-apoptotic genes, such as *Bcl-2*, in microvascular endothelial cells can improve endothelial survival and microvessel stability *in vivo* (Schechner *et al*., 2000). ECs were shown to form functional microvessels when co-seeded with mouse mesenchymal cells in fibronectin–collagen type I protein gels (Koike *et al*., 2004). A functional blood vessel correlates with the transition of a growing vascular network to a quiescent vascular phenotype (Adams and Alitalo, 2007). Our laboratory has previously employed an *in vitro* organotypic vessel co-culture system in order to model vessel maturation (Evensen *et al*., 2009). Endothelial cells co-cultured with mural cells (SMCs or mesenchymal stem cells, MSCs) result in a spontaneous endothelial capillary-like network formation and deposition of a complex basement membrane leading to an endothelial VEGF-independent phenotype. We applied the principles defined by these *in vitro* results to address whether uniform vessel assembly can be accelerated in a physiological *in vivo* tissue-engineering context (Nor *et al*., 2001). Our results emphasize the dominant pro-maturation effect of vascular SMCs that enforces formation of a uniform, branched functional intra-scaffold microvasculature, providing a methodological and conceptual basis for improving tissue-engineering strategies.

2. Materials and methods

2.1. Cells

Human dermal microvascular endothelial cells (HMVECs; single donor lot, Lonza) were grown in EGM-2 MV medium (Lonza). Human pulmonary artery smooth muscle cells (hPASMCs; single donor lot; Lonza) were grown in SmGm medium (Lonza). Primary cells were used at passages 3–7. Phoenix A retroviral packaging cells (ATCC) were grown in Dulbecco's modified Eagle's medium (DMEM), 4500 mg/ml glucose (Sigma-Aldrich) supplemented with 10% fetal bovine serum (FBS; Euro Clone/PAA), 5% penicillin–streptomycin (Sigma-Aldrich) and 5% L-glutamine (Sigma-Aldrich).

2.2. Retroviral transduction

Phoenix A retroviral packaging cells were transfected with GFP or RFP retroviral vectors (Evensen *et al*., 2009) according to Swift *et al*. (1999). Briefly, subconfluent Phoenix A cells were transfected by $CaCl_2$ precipitation in the presence of chloroquine (Sigma-Aldrich). Virus was harvested in EGM-2 MV or SmGm medium 48 h post-transfection and added to subconfluent HMVECs or hPASMCs (passages 3–5) with 5 μg/ml protamine sulphate (Sigma-Aldrich) for 16 h. Transduced GFP-expressing HMVECs and RFP-expressing hPASMCs were purified by flow cytometric sorting on a FACSAria Cell Sorter (BD Biosciences).

2.3. *In vitro* organotypic blood vessel system

A microtitre plate format *in vitro* organotypic blood vessel system assay was conducted as described (Evensen *et al*., 2009). Briefly, 6000 GFP-expressing HMVECs and 50 000 hPASMCs were co-seeded in EGM-2 MV medium in a 96-well plate. Co-cultures were imaged after 72 h, using a fully automated high-throughput fluorescence microscope (BD Pathway 855).

2.4. Experimental animals

For all experiments, non-obese mice with severe combined immunodeficiency disease (NOD/SCID; Gade Institute/Taconic Farms) were used. The animals were aged approximately 6–8 weeks at the time of scaffold implantation. All experiments were approved by the Norwegian Animal Research Authority and conducted according to the European Convention for the Protection of Vertebrates Used for Scientific Purposes.

2.5. Scaffold preparation

Poly-L-lactic acid (PLLA) scaffolds were produced by a solvent-casting particulate-leaching technique, previously described by Nor *et al*. (2001). 1 g PLLA (Resomer L 206 S, Boehringer Ingelheim) was dissolved in 20 ml chloroform (Sigma) to yield a 5% solution. NaCl (Fisher Scientific) was sieved through a test sieve (Retsch) with a pore size of 450 μm, and 3.45 g sieved NaCl was distributed in silanized glass beakers. The NaCl was mixed with the 5% PLLA solution and the solvent was left to evaporate. Thereafter, the scaffolds were leached for 48 h

DOI: 10.1002/term

with double-distilled water to wash out the NaCl, and then dried and cut into $6 \times 6 \times 1$ mm pieces. The scaffolds were sterilized in a descending alcohol series from 100% to 70% EtOH and kept in sterile phosphate-buffered saline (PBS) until implantation.

2.6. Tissue-engineering model

Prior to implantation, the scaffolds were dried briefly on sterile paper and filled with a total of 1×10^6 cells in 36 µl 50 : 50 EGM-2 MV and growth factor-reduced phenol red-free Matrigel (BD). The scaffolds were left at 37 °C for 30 min for the Matrigel to solidify. The scaffolds were seeded with 1×10^6 HMVECs alone, 1 : 1 (500 000 HMVECs:500 000 hPASMCs) or 1 : 4 (200 000 HMVECs:800 000 hPASMCs) ratios. For each experimental group, five mice were implanted with two scaffolds each. Acellular scaffolds containing Matrigel only were implanted into four mice, and scaffolds seeded with 1×10^6 hPASMCs only were implanted into five mice to provide negative controls for histology and imaging.

NOD/SCID mice were anaesthetized with an intramuscular injection of 20 µl 1 : 2 concentration of Rompun (Xylazin; 20 mg/ml; Bayer Health Care):Narketan (Ketamin; 100 mg/ml; Vétoquinol) in the thigh muscle. A 2.5 cm incision was made on the back of the mouse and the scaffolds were placed in skin flaps at the flanks. After 7, 14 or 21 days, the mice were sacrificed by cervical dislocation after deep Isoflurane (Schering-Plough) anaesthesia, and the scaffolds were recovered for fixation.

2.7. Histological staining

The scaffolds were fixed in 10% paraformaldehyde (PFA) and subsequently paraffin-embedded for sectioning. Sections from the middle part of the scaffold were deparaffinized and stained with monoclonal mouse-anti human CD31 (M0823, Dako), and monoclonal mouse anti-human smooth muscle actin (M0851, Dako), visualized with 3,3′-diaminobenzidine tetrahydrochloride (DAB; EnVision™ detection system, K5007, Dako) and counterstained with haematoxylin (DakoREAL™ Haematoxylin S2020, DAKO). Antibody specificity was validated using sections from acellular and hPASMCs-only implants.

2.8. Functional multiphoton fluorescence microscopy analysis

In order to specifically label perfused human endothelial cells in the scaffolds, 200 µl UEA1–lectin–FITC (Sigma-Aldrich; 1 mg/ml in sterile 0.9% NaCl) was injected into the lateral tail vein 30 min before sacrifice (Holland *et al.*, 2005) The scaffolds were excised and immediately imaged using a Multiphoton Microscope (Leica SP5). Acquired serial images were analysed using 3D image analysis software (IMARIS 6.3).

2.9. Flow cytometry analysis

Scaffolds were removed 30 min after injection with UEA1–Lectin–FITC and homogenized using a syringe in a collagenase A solution (Sigma-Aldrich; 22 U/ml). The cells were centrifuged at 1000 rpm for 5 min, washed with PBS and filtered with a 40 µm pore size filter. The cells were then washed once more, resuspended in PBS and analysed by flow cytometry for FITC fluorescence. Propidium iodide staining (1 µg/ml; Molecular Probes) was performed in order to exclude dead cells from the analysis.

2.10. Image analysis

To quantify the number of vessels/mm^2 and the vessel diameter, histological sections of scaffolds were examined with a light microscope (Leica). Using the image-processing program AnalySIS, the outlines of anti-hCD31-staining vessels in five fields of view of a section were encircled manually at ×200 magnification. The number of vessels from five fields of view was used to calculate the vessel diameter and number of vessels/mm^2. Vessels were subdivided into five categories based on diameter, <10, 10–20, 20–30, 30–50 and 50 µm, that are characteristic for capillary arteriole, artery and immature vessels (Silverthorn *et al.*, 2004).

Serial multiphoton fluorescence images acquired from *ex vivo* scaffolds were reconstructed using 3D image analysis software (IMARIS 6.3). The length and the diameter of UEA–lectin–FITC-stained vessels was quantified in images using IMARIS. Analysis of the mean distance between human UEA–lectin–FITC stained vessels and RFP-expressing hPASMCs in the scaffolds was performed as follows. Binary masks of voxels identified as belonging to vessels or smooth muscle cells (green and red in Figure 7A) were exported from IMARIS 6.3 as a series of TIFF images and imported as image stacks into the Fiji distribution of ImageJ (Rasband, 1997–2008). The distance of every voxel to the nearest hPASMC/RFP was calculated by applying the Euclidean distance transformation to the hPASMC/RFP image stack (Dougherty and Kunzelmann, 2007). The distances for the subset of voxels forming the surface of the vessels was obtained by applying the Binary Outline tool to the HMVEC/UEA1–lectin–FITC image stack and using this to mask the Euclidean distance map calculated above. This yielded the distance of each of 159 147 voxels on the vessel surfaces to the nearest hPASMC/RFP voxel.

2.11. Statistics

The statistical significance of the data was evaluated using a one-tailed Student's *t*-test. Statistically significant differences are denoted $^*(p < 0.05)$ or $^{**}(p < 0.01)$. Number (n) in each experiment refers to the number of scaffolds analysed. This number was always 6 or

DOI: 10.1002/term

larger (maximum, $n = 12$) for the immunohistochemistry analysis; for the *ex vivo* imaging, $n = 4$. All values in bar diagrams are presented as mean ± standard error of mean (SEM).

3. Results

3.1. Engineering mature human microvasculature from vascular components *in vivo*

Maturation of nascent blood vessels requires heterotypic vascular cell–cell interactions (Evensen *et al.*, 2009). We analysed a microtitre plate format *in vitro* organotypic blood vessel system, comprising primary HMVECs co-cultured *in vitro* with human pulmonary artery-derived vascular smooth muscle cells (hPASMCs). HMVEC–hPASMC co-cultures form extensive capillary-like networks and deposit a peri-endothelial basement membrane-like structure comprising vascular collagens (Figure 1A–C). To determine whether this vessel self-assembly process can form a functional microvasculature in an *in vivo* tissue engineering context, we developed a tissue-engineering model comprising HMVECs and hPASMCs co-seeded with soluble basement membrane proteins (Matrigel) into a PLLA scaffold that is implanted into the dorsal subcutaneous tissue of an immunodeficient mouse host context (Nor *et al.*, 2001). Subcutaneous PLLA scaffold implants become enveloped by connective tissue within 5 days and anastomose with local host fascial vessels (Nor *et al.*, 2001). The subcutaneous microenviroment is hypoxic and thus is a relevant assessment of microvessel formation efficiency within a tissue-engineering scaffold (Patterson *et al.*, 2008).

PLLA scaffolds were fabricated with ≥450 μm pores and seeded with primary human vascular cells and soluble basement membrane proteins (Figure 2A, B). Primary human vascular cells attached to the PLLA scaffold surface within 24 h (Figure 2C). PLLA scaffolds seeded with HUMVECs in monoculture or HUMVECs and vSMCs at a 1 : 1 or 1 : 4 ratio were implanted subcutaneously into immunocompromised NOD-SCID mice. Implants were retrieved 7, 14 or 21 days post-implantation and evaluated for the presence of intra-scaffold human microvasculature by immunohistochemistry, using anti-human CD31 (Figure 3). Patent vessels stained by anti-human CD31 were evident throughout scaffolds seeded with the complete complement of vascular components 7 days after implantation (Figure 3A). The presence of intralumenal red blood cells within the engineered human microvessels evidenced successful anastomosis with the local fascial vasculature and perfusion by the host circulation (Figure 3A). The intra-scaffold human vasculature was predominately functional at 14 and 21 days, displaying more uniform diameters and intralumenal host-derived red blood cells (Figure 3B, C). No anti-human CD31-staining vessels were detected in sections from acellular or hPASMCs-only scaffold implants (see Supporting information, Figure S1).

To ascertain the localization of the co-seeded hPaSMCs, we conducted immunohistochemical analysis with anti-α-SMC actin (α-SMA) and anti-human CD31 in co-culture experiments with a HMVECs : hPaSMCs ratio of 1 : 4. Tissue sections derived from 7 and 14 day scaffold implants showed that anti-α-SMA staining cells co-localized with patent human CD31-staining vessels, likely representing co-seeded hPASMCs, as these time points precede the invasion of host mural-derived cells (Figure 4A, B) (Nor *et al.*, 2001). The anti-α-SMA staining cells became preferentially perivascular, encircling all scaffold human vessels at 14 and 21 days post-implantation (Figure 4B, C). Hence, co-seeded HMVECs and hPASMCs adopt a native vessel configuration in the *in vivo* tissue-engineering context.

3.2. hPASMCs enhance the formation of small diameter microvessels in tissue-engineering scaffolds

To determine whether vessel self-assembly in the *in vivo* tissue-engineering context enhanced the formation of small-calibre microvessels by the presence of hPASMCs, we co-seeded HMVECs and hPASMCs at different ratios (1 : 1, 1 : 4) or HMVECs alone (1 : 0) into Matrigel-enriched PLLA scaffolds and evaluated vascularization parameters following subcutaneous implantation. Subcutaneous vascular cell implants were retrieved at different time points from the immunodeficient host

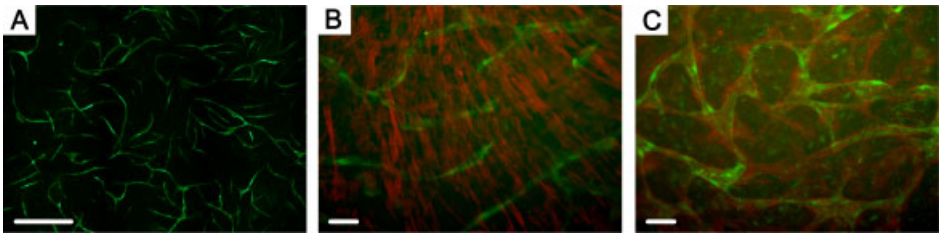

Figure 1. HMVECs and hPASMCs form capillary-like networks *in vitro*. (A) Live cell fluorescence microscopy imaging of a capillary-like network formed by GFP-expressing HMVECs after 5 days in co-culture (1 : 4) with hPASMCs (unlabelled). (B) Localization of hPASMCs (anti-α-SMC/TRITC) in a 5 day co-culture with GFP–HMVECs. (C) Fluorescence microscopy analysis of peri-endothelial collagen XVIII deposition (anti-collagen XVIII/TRITC) in GFP–HMVECs–hPASMCs (unlabelled) 5 day co-culture. Scale bar = 50 μm

DOI: 10.1002/term

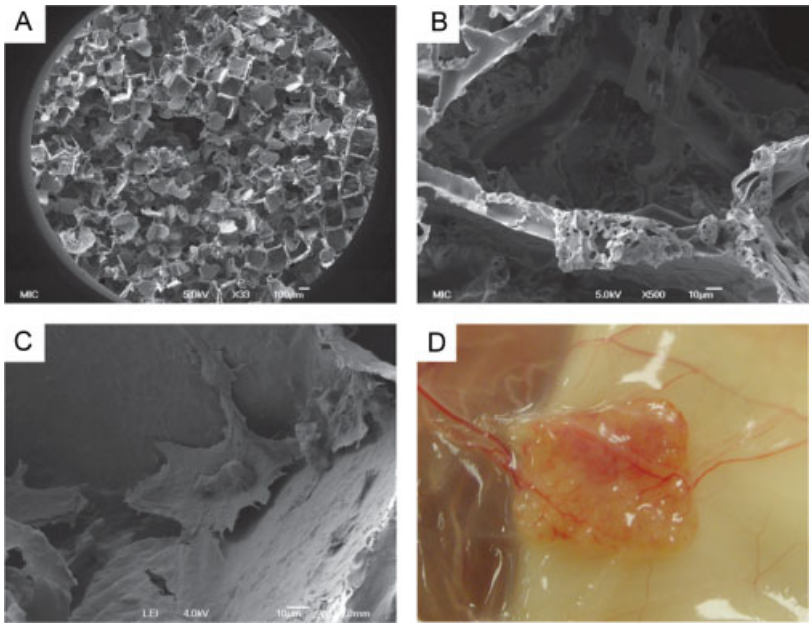

Figure 2. PLLA scaffolds support cell attachment. Biocompatible and biodegradable poly-L-lactic acid (PLLA) scaffolds, produced by a solvent-casting particulate-leaching technique, have a highly porous structure, with an average pore size of 400 μm. Scanning electron microscope images, ×33 (A) and ×500 (B), show the deep pores penetrating the scaffold. (C) PLLA scaffolds support cell attachment, as illustrated by a primary human vascular smooth muscle cell attaching to the wall of a scaffold pore. (D) A subcutaneous PLLA scaffold seeded with human vascular cells 14 days post-implantation

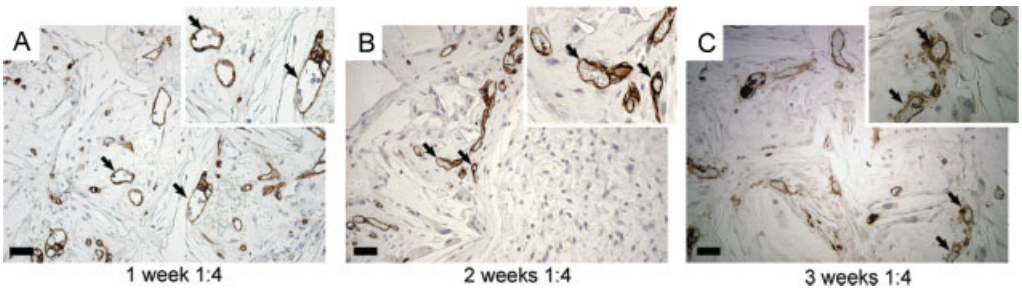

Figure 3. Morphological and immunohistological analysis of scaffold microvasculature development. Scaffold implants were excised at different time points and embedded in paraffin. Tissue sections were stained with anti-human CD31 and haematoxylin. Longitudinal analysis of CD31-staining human microvessels formed within scaffolds seeded with HMVECs and hPASMCs (1 : 4) at (A) 7 days, (B) 14 days and (C) 21 days post-implantation. The presence of intralumenal red blood cells within patent anti-CD31 stained vessels demonstrates that the engineered human microvessels are functional and perfused by the host blood circulation (arrows, inset). Scale bar = 50 μm

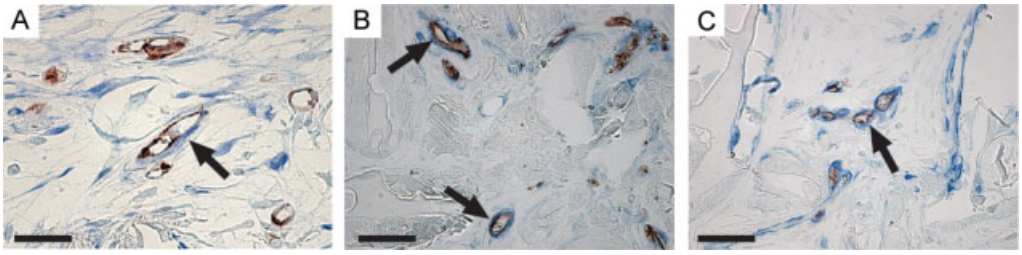

Figure 4. Co-seeded smooth muscle cells are perivascularly localized. Anti-α-smooth muscle cell actin (α-SMA)-stained human hPASMCs (arrows) are co-localized with anti-CD31-stained microvessels in HMVECs/hPASMCs (1 : 4) scaffolds 7 days post-implantation (A). hPASMCs show increased perivascular localization in 14 day (B) and 21 day (C) scaffolds. Scale bar = 50 μm

mice and immunohistochemical morphometric analysis was conducted to measure the human intra-scaffold microvessel number and diameter. Microvessels were assigned to five categories, based on the expected diameter distribution of the microvasculature (Gray, 2004; Jenkins, 2007), <10, 10–20, 20–30, 30–50

DOI: 10.1002/term

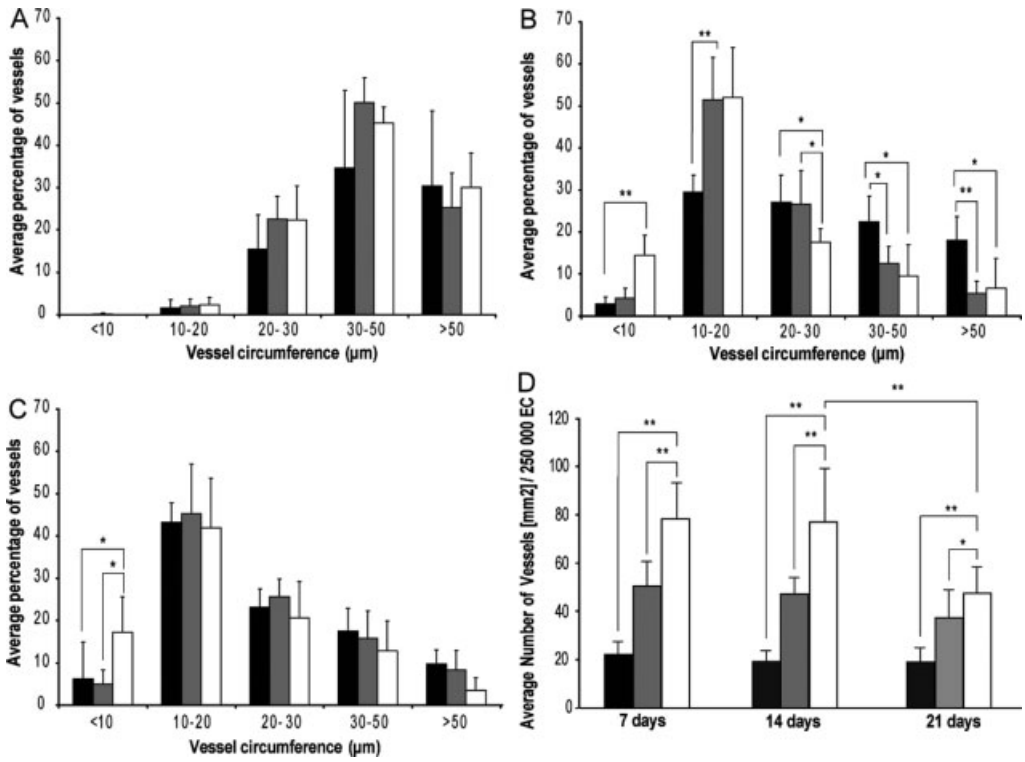

Figure 5. Smooth muscle cells enhance vessel maturation. Morphometric analysis of CD31-staining human microvessels formed in scaffolds seeded with HMVECs only (black bars) or HMVECs–hPASMCs (1 : 1; grey bars) and HMVEC–hPASMCs (1 : 4; (white bars) at 7 days post-implantation (A) show a predominance of 30–50 μm diameter vessels, indicative of a maturing vasculature. After 14 days (B) the CD31-staining human microvessels decreased in calibre. The HMVEC–hPASMC-derived microvessels were mainly 10–20 μm in diameter, representing a mature microvasculature. HMVECs alone remained distributed among larger-calibre microvessels. After 21 days (C), the microvessels in all the scaffolds were predominately 10–20 μm in diameter. The 1 : 4 HMVECs : hPASMCs displayed a much larger percentage of small-calibre vessels. (D) The efficiency of microvascular formation (microvascular density/250 000 HMVECs) was enhanced by the presence of hPASMCs. *$p < 0.05$; **$p < 0.01$

and >50 μm, where vessels >50 μm were defined as immature vessels and vessels <10 μm and 10–20 μm were defined as mature microvasculature. The remaining size groups were defined as transitional. Analysis of 7 day scaffolds showed that the vessels were mainly 30–50 μm in diameter in all three vascular implants, indicative of maturing, transitional microvasculature (Figure 5A). At 14 days post-implantation, the intra-scaffold microvasculature formed from the complete sets of vascular components showed a strong shift in the vessel size distribution to predominately 10–20 μm diameter microvessels, indicative of vessel maturation (Figure 5B). The co-seeded HMVECs : hPASMCs (1 : 4) group showed an increased proportion of <10 μm diameter microvessels, demonstrating a greater degree of capillary-calibre vessels (Figure 5B). This microvessel distribution remained unchanged in the third week (Figure 5C) for co-seeded implants. In contrast, implants lacking hPASMCs did not show a commensurate microvessel size distribution shift until 21 days post-implantation, corresponding to the invasion of host mural cells (Nor *et al*., 2001). Notably, the efficiency of intra-scaffold microvascular formation (microvascular density per seeded EC) in the HMVEC : hPASMC (1 : 1 and 1 : 4) co-seeded scaffolds was enhanced 2.5- and four-fold relative to HMVECs alone at day 14 (Figure 5D). This is somewhat reduced at day 21, likely reflecting perfusion-mediated vascular remodelling. Collectively, these results indicate that a complete complement of vascular components stimulates the rapid formation and maturation of uniform small-calibre microvessels in a tissue-engineering context *in vivo*.

3.3. Analysis of tissue-engineered functional microvasculature by fluorescence angiography

In order to functionally evaluate the intra-scaffold microcirculation engineered with the complete complement of vascular components, we conducted a fluorescence angiography analysis. UEA1–lectin conjugated to FITC, which binds specifically to mannose moieties on the luminal surface of human endothelial cells, was injected into the host mouse circulation 30 min prior to sacrifice. To determine the presence of UEA1–lectin–FITC-stained HMVECs that manifest an intra-scaffold microcirculation, we interrogated cells harvested from excised 14-day scaffolds by flow cytometry. A large population of UEA1–lectin–FITC-stained cells were apparent in the green fluorescence channel. These perfused human endothelial cells exhibited high forward light scatter values, indicating that larger, potentially elongated

DOI: 10.1002/term

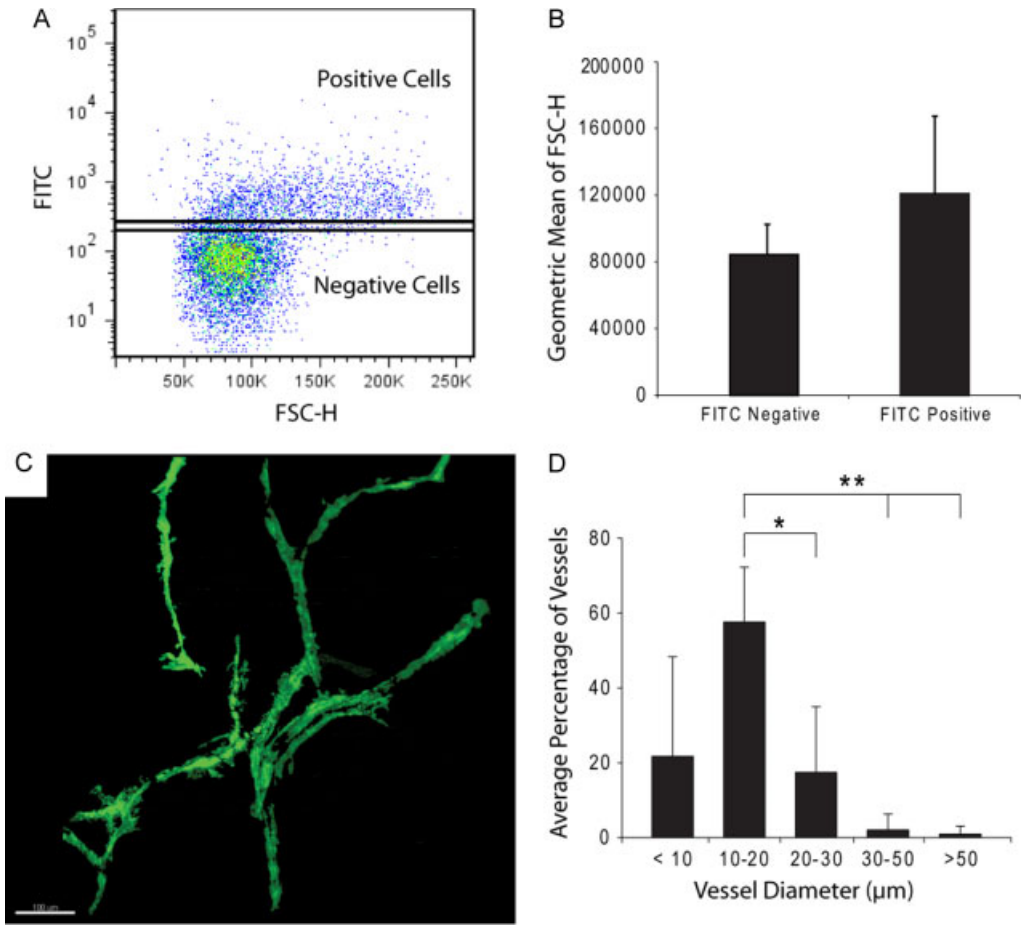

Figure 6. Functional analysis of scaffold microcirculation by fluorescence angiography. Animals were injected at 14 days post-implantation with UEA–lectin–FITC 30 min prior to scaffold recovery to selectively label perfused human endothelial cells. (A) Bivariate flow cytometry analysis of cells harvested from scaffolds. UEA–lectin–FITC fluorescence-positive cells (upper box) correlated with higher forward light scatter (FSC) relative to non-staining cells (lower box). (B) Mean forward light scatter (FSC) values of perfused UEA–lectin–FITC fluorescence-positive HMVECs vs non-staining cells. (C) Multiphoton fluorescence microscopy image analysis (IMARIS) of perfusion-labelled UEA1–lectin–FITC human microvasculature within a 14 day scaffold shows extensive branching of uniform microvessels. (D) Morphometric analysis of UEA1–lectin–FITC-stained human microvessels from four independent experiments shows that functional microvessels were predominately 10–20 μm in diameter

endothelial cells comprise the functional microvasculature (Figure 6A, B) (Ohnuma *et al.*, 2006). In order to further investigate the morphology of the perfused vessels, we conducted a morphometric analysis of the UEA1–lectin–FITC-stained human vessels in scaffolds by multiphoton fluorescence microscopy. A series of fluorescence images were collected from 100 μm inside vascularized scaffolds and reassembled by 3D image analysis to determine the length and diameter of individual vessel branches of the functional microvasculature. This UEA–lectin–FITC angiography analysis revealed the presence of an extensive branched network of perfused human microvessels within scaffolds implanted for 14 days (Figure 6C). No UEA–lectin–FITC-staining was detectable within 14 day acellular scaffolds or peripheral mouse fascial vessels (see Supporting information, Figure S1). The UEA–lectin–FITC-stained human endothelial cells displayed abundant filapodia, consistent with ongoing vessel remodelling. The perfused human vessels were measured to be predominately <20 μm in diameter, in accordance with the immunohistochemistry analysis (Figures 5, 6D). Hence, tissue-engineering implants comprising a complete complement of vascular components effectively self-assemble into a functional intra-scaffold microvasculature that establishes a microcirculation with the host.

In order to compare the location of the hPASMCs relative to the perfused microvessels within the scaffold, we studied scaffolds seeded with HMVECs and RFP-expressing hPASMCs (hPASMC/RFP). After 2 weeks, mice carrying HMVEC–hPASMC/RFP-seeded scaffolds were injected with UEA–lectin–FITC. Following excision, the scaffolds were analysed for the presence of RFP-expressing hPASMCs and UEA–lectin–FITC-stained human endothelial cells by multiphoton fluorescence microscopy at 100 μm depths. 3D image reconstruction from multiphoton microscopy 3D image stacks revealed that the majority of the hPASMC/RFP are located near the perfused endothelial cells (Figure 7A, B). To quantitate this, volumetric pixel analysis of the 3D-image stacks was performed. The analysis showed that the hPASMCs were closer to the perfused endothelial cells

DOI: 10.1002/term

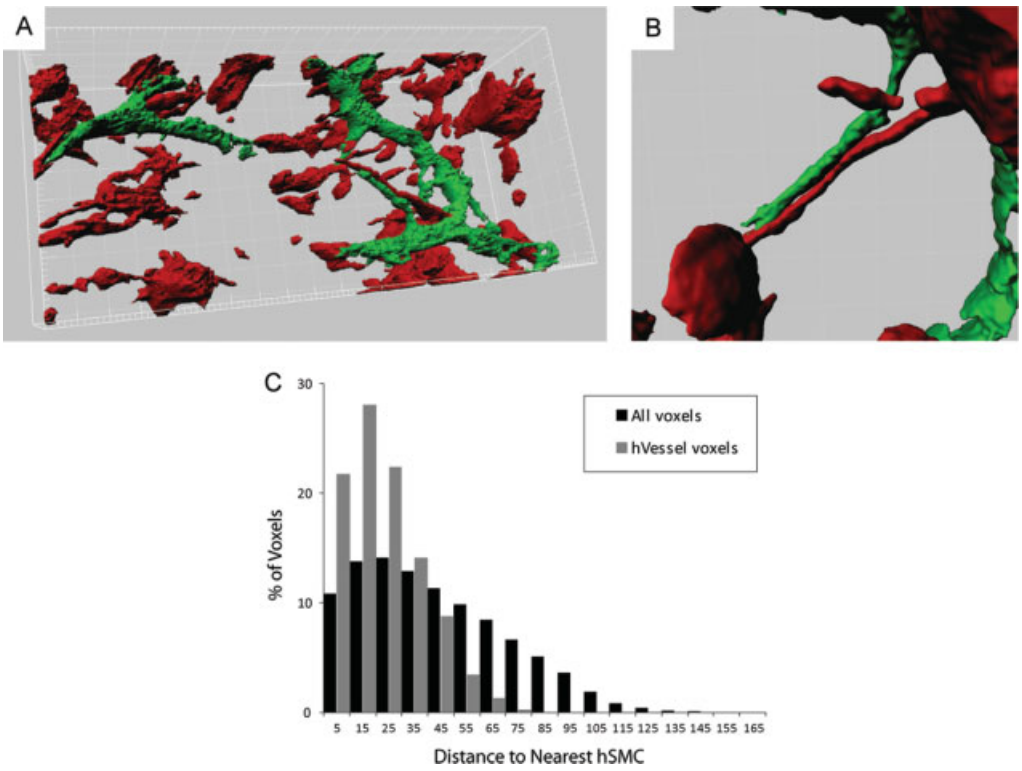

Figure 7. Perfused vessels preferentially co-localize with smooth muscle cells within the scaffold. (A) Multiphoton fluorescence microscopy 3D image analysis (IMARIS) of RFP-expressing hPASMCs and UEA1–lectin–FITC-stained human microvessels within a 14 day scaffold. (B) Implanted RFP-expressing hPASMCs were frequently perivascularly localized. (C) Distribution of distances (determined by Euclidean distance transformation) to the nearest hPASMC/RFP (red channel voxel) from functional UEA1–lectin–FITC-stained human microvessels (green channel voxel) and all voxels within the 3D image. The measured mean distance between perfused vessels and hPASMCs (22.6 ± 14.6 μm) was significantly smaller than would be expected for randomly distributed vessels (43.1 ± 0.07 μm); $p < 0.00001$

than would be expected for a random distribution, indicating co-localization (Figure 7C). hPASMC/RFP and UEA1–lectin–FITC voxels within multiphoton microscopy 3D image stacks were separated by a mean distance of 22.6 ± 14.6 μm vs an expected random distribution mean of 43.1 ± 0.07 μm ($p < 0.0001$). This is consistent with the notion that hPASMCs enhance vessel maturation in the tissue-engineering context by juxtapositional heterotypic cell–cell interactions and paracrine signalling.

4. Discussion

A current challenge facing tissue-engineering approaches is the expedient establishment of a microcirculation to meet the metabolic needs of the developing tissue implants and avoid cell death. We demonstrate here that efficient self-assembly of a functional microvasculature can be achieved in a physiological *in vivo* tissue-engineering implant by providing individual vascular cellular and basement membrane components. In particular, our results emphasize the critical role of vascular mural cells in enforcing generation of a uniform, branched functional microvasculature in a tissue-engineering context.

The recruitment of mural cells to the abluminal surface of nascent blood vessels is a key prerequisite for vessel maturation (Jain, 2003). Mural cells define a context comprising heterotypic cell–cell, cell–ECM deposition contacts and juxtacrine growth factor receptor signalling that regulate endothelial cell proliferation and survival (Adams and Alitalo, 2007; Beck and D'Amore, 1997; Carmeliet, 2003; Darland and D'Amore, 2001; Gaengel *et al*., 2009; Hellstrom *et al*., 2001; Jain, 2003; Korff *et al*., 2001). Proper growth factor receptor crosstalk between EC–mural cells also engenders local vascular basement membrane deposition required for vessel maturation and stability (Davis and Senger, 2005). This perivascular microenviroment serves an important role in delimiting endothelial responses to pro-angiogeneic factors emanating from the local tissue (Jain, 2003). Organotypic endothelial–vSMC co-culture models demonstrate that paracrine mural cell-derived VEGF is crucial to endothelial capillary-network-like formation and that mural cell Ang-1 regulates endothelial responsiveness to tissue-derived VEGF (Evensen *et al*., 2010; Korff *et al*., 2001). This switch from tissue-derived to mural cell-derived VEGF likely promotes vessel maturation, ultimately leading to VEGF independence and reduced vessel plasticity (Benjamin *et al*., 1998; Darland and D'Amore, 2001). Importantly, recent studies show that dysregulated tissue VEGF levels can affect mural cell functions and inhibit vessel maturation (Greenberg *et al*., 2008).

Several previous studies have reported that mural cell types enhance the stability of endothelial cells and the formation of functional vessels in tissue implants (Au *et al.*, 2008; Koike *et al.*, 2004; Melero-Martin *et al.*, 2007; Shepherd *et al.*, 2009). Congruently, we demonstrate that the efficiency of intra-scaffold microvascular formation was enhanced by the presence of vascular smooth muscle cells. Indeed, a 1 : 4 EC : mural cell ratio of vascular progenitor cells also generated the greatest vessel density within Matrigel implants (Melero-Martin *et al.*, 2008) A further critical role of perivascular cells is to enforce diametral uniformity in branched microvascular networks (Evensen *et al.*, 2009; Gerhardt and Betsholtz, 2003). Genetic and pharmacological inhibition of mural cell recruitment to growing vessels and is associated with exacerbated angiogenesis and endothelial hypertrophy that form irregular, enlarged vessels and aneurysms (Hellstrom *et al.*, 2001; Wilkinson-Berka *et al.*, 2004). Mural cells exert vessel morphogenic control both via modulating endothelial cell signalling responses and contractile vasoconstriction that collectively regulate haemodynamic parameters (Gaengel *et al.*, 2009; Gerhardt and Betsholtz, 2003). Thus, to study vascularization in the tissue-engineering setting, it is important to employ imaging approaches to facilitate interrogation of the perfused microvascular branched network architecture (Au *et al.*, 2008; McDonald and Choyke, 2003; Sanz *et al.*, 2008). To address this aspect, we utilized functional multiphoton microscopy to selectively image the engineered microcirculation. The acquisition of multiple, stacked images from functionally labelled scaffold implants facilitates imaged-based 3D reconstruction and quanitification of spatial perivessel cellular relationships. Analysis of 3D image reconstructions demonstrated that hPASMCs preferentially co-localized with perfused vessels. This is congruent with a previous study, where intra-vital multiphoton microscopy through cranial windows showed that co-implanted mesenchymal stem cells acquired smooth muscle cell traits and preferentially co-localized with perfused HUVECs (Au *et al.*, 2008). Together, these results highlight the requisite role of proper spatial mural–endothelial cell interactions in achieving a vascularized tissue-engineering implant.

Earlier studies have demonstrated that increasing local concentrations of VEGF in ischaemic tissues correlated with increased vessel density but did not predict improved tissue blood flow (Ozawa *et al.*, 2004; von Degenfeld *et al.*, 2006). Instead, uniformity of vessel diameters was the most important predictor of enhanced circulation, emphasizing that vessel density measurements are insufficient predictors of angiogenic efficiency. Using functional multiphotonic image analysis, we demonstrated that the microcirculation within hPASMC/HMVEC implants preferentially comprised highly branched, uniform small-calibre vessels (<20 μm). In contrast, a recent study that used Bcl-2-expressing human umbilical cord endothelial cells (HUVECs) seeded in poly(glycolic acid) (PGA) scaffold-supported protein gels found that co-engraftment of hPASMCs led to an increase in large-calibre (>50 μm) vessels (Shepherd *et al.*, 2009). Hence, various combinations of heterogeneous vascular cells can retain a propensity to form vessels of diverse sizes (Garlanda and Dejana, 1997). These results emphasize the importance of using functional morphometric imaging modalities to interrogate engineered vessels formed by clinically amenable endothelial and mesenchymal progenitor cells that can acquire a spectrum of differentiated characteristics (Au *et al.*, 2008; Melero-Martin *et al.*, 2007, 2008).

We conducted our experiments with native, early-passage human vascular cells in the context of one of the few FDA-approved (PLLA) tissue-engineering scaffolds for medical implantation purposes (Freeman, 2007; Yun Chen, 2006). In order to promote initial cell attachment, we prepared scaffold implants with Matrigel-derived ECM proteins (laminin, collagen IV, entactin and heparin sulphate proteoglycan). Using scanning electron microscopy, we show that vascular cells can productively adhere to the scaffold surface under these conditions. The use of a scaffolding material and ECM gel provides a biocompatible porous skeleton for cell attachment, and therefore functions as a temporary ECM for the implanted cells. The combination of PLLA and an ECM protein gel comprises an engineered microenvironment that is optimal for many applications, particularly where resistance to compression or contraction is important, and serves as a model for evaluating new cellular combinations for tissue development (Shepherd *et al.*, 2009).

In a recent study, we applied these concepts to develop a tissue engineering-based tumour model to enable evaluation of tumour–vasculature interactions (Gjerdrum *et al.*, 2010). Tricellular tumour implants comprising human breast carcinoma, primary microvascular endothelial and vascular smooth muscle cells co-seeded into Matrigel-enriched PLLA scaffolds formed highly vascularized tumours. Interestingly, the presence of a functional engineered microvasculature at 2 weeks post-implantation corresponded with enhanced tumour growth rate. However, in contrast to the present study, only large-calibre diameter vessels were formed (>80 μm). These results exemplify how tissue-engineering approaches developed for regenerative medicine applications afford new opportunities to improve models of disease.

5. Conclusion

The efficient self-assembly of a functional microvasculature in an *in vivo* tissue engineering context from individual vascular components defines a conceptual basis for improving contemporary tissue-engineering approaches. The combination of immunohistochemical, flow-cytometric and multiphotonic image analysis provides a methodological foundation for improved evaluation of vascular parameters in bioengineered tissues.

DOI: 10.1002/term

Acknowledgements

We thank Gerd Lillian Hallseth, Bendik Nordanger, Sissel Vik Berge, Marianne Enger and Paula Ruurs for excellent technical assistance. This work was supported by the University of Bergen (fellowships to A.H., C.T. and M.H.), the Norwegian Research Council (Grant Nos 183850 and 183775 to J.B.L.) and the National Institutes of Health (Grant Nos P50-CA97248 and R21-DE19279 to J.E.N.).

Supporting information on the internet

The following supporting information may be found in the online version of this article:

Figure S1. Specificity controls.

References

Adams RH, Alitalo K. 2007; Molecular regulation of angiogenesis and lymphangiogenesis. *Nat Rev Mol Cell Biol* **8**: 464–478.

Alajati A, Laib AM, Weber H, *et al*. 2008; Spheroid-based engineering of a human vasculature in mice. *Nat Methods* **5**: 439–445.

Au P, Tam J, Fukumura D, *et al*. 2008; Bone marrow-derived mesenchymal stem cells facilitate engineering of long-lasting functional vasculature. *Blood* **111**: 4551–4558.

Beck L Jr, D'Amore PA. 1997; Vascular development: cellular and molecular regulation. *FASEB J* **11**: 365–373.

Benjamin LE, Hemo I, Keshet E. 1998; A plasticity window for blood vessel remodelling is defined by pericyte coverage of the preformed endothelial network and is regulated by PDGF-B and VEGF. *Development* **125**: 1591–1598.

Black AF, Berthod F, L'Heureux N, *et al*. 1998; *In vitro* reconstruction of a human capillary-like network in a tissue-engineered skin equivalent. *FASEB J* **12**: 1331–1340.

Black AF, Hudon V, Damour O, *et al*. 1999; A novel approach for studying angiogenesis: a human skin equivalent with a capillary-like network. *Cell Biol Toxicol* **15**: 81–90.

Carmeliet P. 2003; Angiogenesis in health and disease. *Nat Med* **9**: 653–660.

Darland DC, D'Amore PA. 1999; Blood vessel maturation: vascular development comes of age. *J Clin Invest* **103**: 157–158.

Darland DC, D'Amore PA. 2001; Cell–cell interactions in vascular development. *Curr Top Dev Biol* **52**: 107–149.

Davis GE, Senger DR. 2005; Endothelial extracellular matrix: biosynthesis, remodeling, and functions during vascular morphogenesis and neovessel stabilization. *Circ Res* **97**: 1093–1107.

Dougherty RP, Kunzelmann K-H. 2007; Local Thickness plugin; computing local thickness of 3D structures with ImageJ. Microscopy and Microanalysis 2007 Meeting, 5–9 August 2007, Fort Lauderdale, FL: www.optinav.com/LocalThicknessEd.pdf.

Evensen L, Micklem DR, Blois A, *et al*. 2009; Mural cell associated VEGF is required for organotypic vessel formation. *PLoS One* **4**: e5798.

Evensen L, Micklem DR, Link W, *et al*. 2010; A novel imaging-based high-throughput screening approach to anti-angiogenic drug discovery. *Cytometry A* **77**: 41–51.

Freeman JW, Woods MD, Laurencin CT. 2007; Tissue engineering of the anterior cruciate ligament using a braid-twist scaffold design. *J Biomech* **40**: 2029–2036.

Gaengel K, Genove G, Armulik A, *et al*. 2009; Endothelial–mural cell signaling in vascular development and angiogenesis. *Arterioscler Thromb Vasc Biol* **29**: 630–638.

Garlanda C, Dejana E. 1997; Heterogeneity of endothelial cells. Specific markers. *Arterioscler Thromb Vasc Biol* **17**: 1193–1202.

Gerhardt H, Betsholtz C. 2003; Endothelial–pericyte interactions in angiogenesis. *Cell Tissue Res* **314**: 15–23.

Gjerdrum C, Tiron C, Hoiby T, *et al*. 2010; Axl is an essential epithelial-to-mesenchymal transition-induced regulator of breast cancer metastasis and patient survival. *Proc Natl Acad Sci USA* **107**: 1124–1129.

Gray H, Bannister LH, Dyson M, *et al*. 2004; *Gray's Anatomy: the Anatomical Basis of Medicine and Surgery*. Churchill-Livingstone: Edinburgh.

Greenberg JI, Shields DJ, Barillas SG, *et al*. 2008; A role for VEGF as a negative regulator of pericyte function and vessel maturation. *Nature* **456**: 809–813.

Hall AP. 2006; Review of the pericyte during angiogenesis and its role in cancer and diabetic retinopathy. *Toxicol Pathol* **34**: 763–775.

Hellstrom M, Gerhardt H, Kalen M, *et al*. 2001; Lack of pericytes leads to endothelial hyperplasia and abnormal vascular morphogenesis. *J Cell Biol* **153**: 543–553.

Holland SJ, Powell MJ, Franci C, *et al*. 2005; Multiple roles for the receptor tyrosine kinase axl in tumor formation. *Cancer Res* **65**: 9294–9303.

Jain RK. 2003; Molecular regulation of vessel maturation. *Nat Med* **9**: 685–693.

Jenkins GW, Kemnitz CP, Tortora GJ. 2007; *Anatomy and Physiology*. Wiley: New York.

Kaully T, Kaufman-Francis K, Lesman A, *et al*. 2009; Vascularization – the conduit to viable engineered tissues. *Tissue Eng Part B Rev* **15**: 159–169.

Koike N, Fukumura D, Gralla O, *et al*. 2004; Tissue engineering: creation of long-lasting blood vessels. *Nature* **428**: 138–139.

Korff T, Kimmina S, Martiny-Baron G, *et al*. 2001; Blood vessel maturation in a three-dimensional spheroidal coculture model: direct contact with smooth muscle cells regulates endothelial cell quiescence and abrogates VEGF responsiveness. *FASEB J* **15**: 447–457.

Kutcher ME, Herman IM. 2009; The pericyte: cellular regulator of microvascular blood flow. *Microvasc Res* **77**: 235–246.

Lazarous DF, Shou M, Scheinowitz M, *et al*. 1996; Comparative effects of basic fibroblast growth factor and vascular endothelial growth factor on coronary collateral development and the arterial response to injury. *Circulation* **94**: 1074–1082.

McDonald DM, Choyke PL. 2003; Imaging of angiogenesis: from microscope to clinic. *Nat Med* **9**: 713–725.

Melero-Martin JM, De Obaldia ME, Kang SY, *et al*. 2008; Engineering robust and functional vascular networks *in vivo* with human adult and cord blood-derived progenitor cells. *Circ Res* **103**: 194–202.

Melero-Martin JM, Khan ZA, Picard A, *et al*. 2007; *In vivo* vasculogenic potential of human blood-derived endothelial progenitor cells. *Blood* **109**: 4761–4768.

Muschler GF, Nakamoto C, Griffith LG. 2004; Engineering principles of clinical cell-based tissue engineering. *J Bone Joint Surg Am* **86A**: 1541–1558.

Nguyen LL, D'Amore PA. 2001; Cellular interactions in vascular growth and differentiation. *Int Rev Cytol* **204**: 1–48.

Nor JE, Peters MC, Christensen JB, *et al*. 2001; Engineering and characterization of functional human microvessels in immunodeficient mice. *Lab Invest* **81**: 453–463.

Ohnuma K, Yomo T, Asashima M, *et al*. 2006; Sorting of cells of the same size, shape, and cell cycle stage for a single cell level assay without staining. *BMC Cell Biol* **7**: 25.

Ozawa CR, Banfi A, Glazer NL, *et al*. 2004; Microenvironmental VEGF concentration, not total dose, determines a threshold between normal and aberrant angiogenesis. *J Clin Invest* **113**: 516–527.

Patterson TE, Kumagai K, Griffith L, *et al*. 2008; Cellular strategies for enhancement of fracture repair. *J Bone Joint Surg Am* **90**(suppl 1): 111–119.

Rasband WS. 1997–2008; ImageJ. In *Health*. USNIO: Bethesda, MD, USA.

Sanz L, Santos-Valle P, Alonso-Camino V, *et al*. 2008; Long-term *in vivo* imaging of human angiogenesis: critical role of bone marrow-derived mesenchymal stem cells for the generation of durable blood vessels. *Microvasc Res* **75**: 308–314.

Schechner JS, Nath AK, Zheng L, *et al*. 2000; *In vivo* formation of complex microvessels lined by human endothelial cells in an immunodeficient mouse. *Proc Natl Acad Sci USA* **97**: 9191–9196.

Shepherd BR, Jay SM, Saltzman WM, *et al*. 2009; Human aortic smooth muscle cells promote arteriole formation by

coengrafted endothelial cells. *Tissue Eng A* **15**: 165–173.
Silverthorn DU, William CO, Garrison CW, *et al*. 2004; *Human Physiology – An Integrated Approach*. Daryl Fox: San Francisco, CA.
Swift S, Lorens J, Achacoso P, *et al*. 1999; Rapid production of retroviruses for efficient gene delivery to mammalian cells using 293T cell-based systems. *Curr Protoc Immunol* 10.17.14–10.17.29.
Von Degenfeld G, Banfi A, Springer ML, *et al*. 2006; Microenvironmental VEGF distribution is critical for stable and functional vessel growth in ischemia. *FASEB J* **20**: 2657–2659.
Wenger A, Kowalewski N, Stahl A, *et al*. 2005; Development and characterization of a spheroidal coculture model of endothelial cells and fibroblasts for improving angiogenesis in tissue engineering. *Cells Tissues Organs* **181**: 80–88.
Wilkinson-Berka JL, Babic S, De Gooyer T, *et al*. 2004; Inhibition of platelet-derived growth factor promotes pericyte loss and angiogenesis in ischemic retinopathy. *Am J Pathol* **164**: 1263–1273.
Yun Chen AFTM, Min W, Jiashen L, *et al*. 2006; PLLA scaffolds with biomimetic apatite coating and biomimetic apatite/collagen composite coating to enhance osteoblast-like cells attachment and activity. *Surf Coat Tech* **201**: 575–580.

DOI: 10.1002/term